Characteristics and diagnostics of an ultrahigh vacuum compatible laser ablation source for crossed molecular beam experiments

Xibin Gu, Ying Guo, Ed Kawamura, and Ralf I. Kaiser[a)]
Department of Chemistry, University of Hawai'i at Manoa, Honolulu, Hawaii 96822

(Received 10 November 2005; accepted 20 March 2006; published 20 April 2006)

We present the design and the characteristics of an ultrahigh vacuum compatible laser ablation source which can be operated in a crossed molecular beam machine at pressures as low as 10^{-9} Torr. This unit provides intense supersonic beams of up to 3×10^{13} cm^{-3} reactant species (carbon atoms, dicarbon, and tricarbon) in the interaction region of a crossed molecular beam machine. Practical delay time windows between the pulsed valve releasing the seeding gas and the laser have been determined to be between 16 630 and 16 645 μs, i.e., firing the laser 150–165 μs after the 80 μs pulsed valve trigger. The concentration of the dicarbon and tricarbon clusters can be maximized/minimized by adjusting the laser focus (a tighter laser focus leads to an enhanced atomic carbon component) and the laser power (multiphoton dissociation). We achieved stable peak velocities between 800 and 3800 m s^{-1} and speed ratios S of up to 6. © *2006 American Vacuum Society.*
[DOI: 10.1116/1.2194935]

I. INTRODUCTION

The energetics and dynamics of reactions of small carbon molecules are of paramount importance in understanding combustion processes[1,2] and the chemical vapor deposition (CVD) of diamonds.[3] Reactive collisions of dicarbon, $C_2(X\,^1\Sigma_g^+/a\,^3\Pi_u)$, and tricarbon molecules, $C_3(X\,^1\Sigma_g^+)$, with unsaturated hydrocarbons are of particular pertinence in unraveling the formation of polycyclic aromatic hydrocarbons (PAHs), their hydrogen deficient precursors, and of carbonaceous nanostructures from the "bottom up."[4] Carbonaceous nanoparticles are commonly referred to as soot and are often associated with incomplete combustion processes.[5] Soot is primarily composed of nanometer-sized stacks of planar layers of carbon atoms. These layers can be characterized as fused benzene rings and are likely formed via agglomeration of polycyclic aromatic hydrocarbons.[6] Once liberated into the ambient environment, soot particles in respirable size of 10–100 nm can be transferred into the lungs by inhalation and are strongly implicated in the degradation of human health,[7] particularly due to their high carcinogenic risk potential. PAHs and carbonaceous nanoparticles are also serious water pollutants and bioaccumulate in the fatty tissue of living organisms. Together with leafy vegetables, where PAHs and soot deposit easily, they have been further linked to food poisoning, liver lesions, and tumor growth.[7] Even smaller soot particles of 1–10 nm can be transported to high altitudes and influence the atmospheric chemistry.[8] These particles act as condensation nuclei for water ice, accelerate the degradation of ozone, and could lead ultimately to an increased rate of skin cancer on Earth and possibly to a reduced harvest of crops. The crucial role of nanodiamonds in chemical vapor deposition on the industrial scale should be also noted.[3]

But despite the key role of carbonaceous nanostructures and their hydrogen deficient precursors in combustion processes (polycyclic aromatic hydrocarbons and soot particles) and chemical vapor deposition (diamonds), the fundamental question "How are these nanoparticles and their precursors actually formed?" has not been conclusively resolved. The majority of mechanistic information on the growth processes has been derived from chemical reaction networks which actually model the formation of, for instance, PAH-like structures in combustion flames.[1,4] These models suggest that the synthesis of small carbon-bearing molecules together with their radicals is linked to the formation of PAHs and to the production of soot and possibly fullerenes in hydrocarbon flames. Various mechanisms have been postulated; those currently in favor are thought to involve a successive buildup of hydrogen deficient carbon-bearing radicals and molecules via sequential addition steps of small hydrogen deficient species (C_2, C_2H, C_3, C_3H, C_3H_2, and C_3H_3) and reactions via acetylene (C_2H_2), PAH-like structures, and fullerenes.[9–11]

Among these reactions, particular attention has been devoted to understand bimolecular collisions of small carbon molecules and to incorporate these data into combustion and chemical vapor deposition models. Dicarbon and tricarbon are the simplest representatives of bare carbon molecules. Both species have been identified in high temperature combustion flames under fuel-rich conditions of incipient soot formation at concentrations near 10^{15} cm^{-3}.[12] These processes were suggested to convert unsaturated hydrocarbons to larger, hydrogen deficient hydrocarbon radicals, which play an important role in soot formation.[13] Note that the crucial role of the dicarbon molecule to build up fullerenes and nanotubes via a stepwise incorporation of C_2 has also been pointed out.[14] Reactions of dicarbon and tricarbon are also important in chemical vapor deposition processes of nanodiamonds.[15] Although current models favor the methyl radical as the key growth species in low power reactors,[16] recent spectroscopic investigations of CVD environments

a)Electronic mail: kaiser@gold.chem.hawaii.edu

detected dicarbon molecules via laser induced fluorescence and by degenerate four wave mixing. More complex species such as C_4H_2, C_4H_3, and C_4H_4 isomers of hitherto unknown origin were further identified in diamond formation processes.[17] Very recently, Goyette *et al.* suggested that dicarbon is the actual precursor in the formation of nanocrystalline diamond;[18] number densities in a $H_2/Ar/CH_4$ plasma have been determined in the order of 10^{13} cm^{-3}. These processes are closely related to the growth of carbon clusters in carbon-rich stars[19] as well as to the synthesis of diamonds in hydrogen-poor preplanetary nebulae[20] and in our solar system.[21]

Due to the importance of the reactions of dicarbon molecules with unsaturated hydrocarbons, it is crucial to elucidate the reaction dynamics of these species. The crossed molecular beam technique represents the most versatile approach in the illumination of the energetics and chemical dynamics of elementary reactions. In contrast to bulk experiments, where reactants are mixed, the main advantage of a crossed beam approach is the capability to form the reactants in separate, supersonic beams. In principle, both reactant beams can be prepared in well-defined quantum states before they cross at a specific collision energy under single collision conditions. The species of each beam are made to collide only with the molecules of the other beam, and the products formed fly undisturbed towards the detector. This implies that the reactant of one beam will collide only with the reactant molecules of a second beam at a specific collision energy and crossing angle, therefore ensuring the observation of the consequences of well-defined molecular encounters. However, the generation of an intense beam of the highly reactive and commercially not available dicarbon molecule presents a tricky problem. In this article, we present the design and the characteristics of a pulsed laser ablation source to generate an intense beam of small carbon clusters of dicarbon and tricarbon. Compared to previous designs,[22,23] this unit is ultrahigh vacuum (UHV) compatible, produces more intense (by a factor of 3–4) beams of dicarbon and tricarbon, and generates beams with a highly reproducible peak velocity and fluctuations of only ±1% on a day-to-day basis.

II. DESIGN OF THE ABLATION SOURCE

The center piece of the ablation source is machined aluminum block ($30\times40\times300$ mm^3) interfaced to the main frame of the carbons source ($50\times50\times350$ mm^3) (Fig. 1). A carbon rod of 70.0 mm in length and an outer diameter of 1.0 cm is located 0.05 mm inside the extension channel of a homemade pulsed piezovalve.[24] The latter extends 8.0 mm downstream from the valve and intersects the laser entrance hole perpendicularly. The laser beam strikes the carbon rod which is interfaced to a motor mike (SP18074-3606). Compared to an earlier design,[22] this motor mike is lubricated with perfluoroether grease (Braycote) and the housing Teflon coated; this guarantees vacua in the primary source region of the crossed beams machine of a few 10^{-9} Torr. The rotational direction of the carbon rod is reversed by an automatic voltage switcher box located outside the vacuum system.

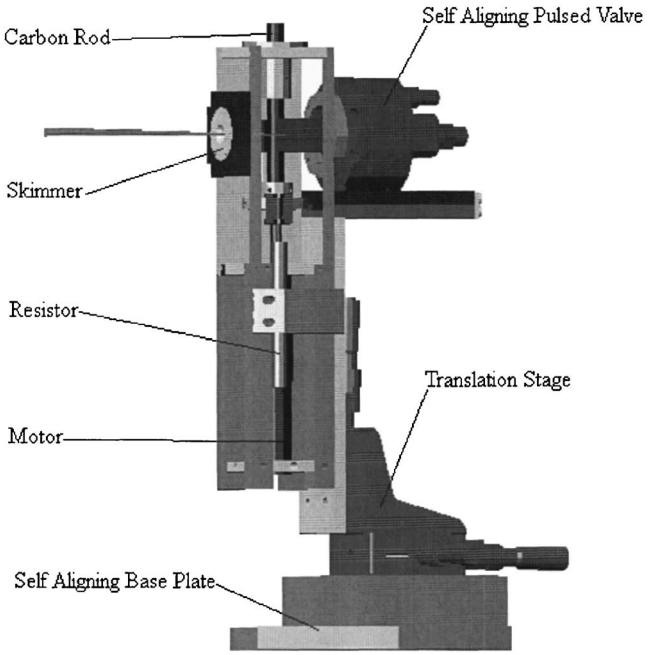

FIG. 1. Three dimensional composite drawings of the laser ablation source in the primary source region together with the skimmer (the differential wall is omitted for clarity).

This device has two set points which encode the polarity switch through a linear potentiometer (variable resistor). The ablation source is interfaced to an *x-y-z* translation stage which in turn is placed on a self-aligning dovetail slide. This construction enables us to replace the carbon rod once every three weeks without realigning the ablation source and the pulsed valve.

III. INCORPORATION OF THE ABLATION SOURCE INTO A CROSSED BEAM MACHINE

The optimization and characterization of the ablation source are carried out in a crossed molecular beam machine. Briefly, the main chamber consists of a 2300 l stainless steel box and is evacuated by three 2000 l s^{-1} magnetically suspended turbo molecular pump backed by a scroll pump (10 l s^{-1}) to the low 10^{-8} Torr region. To reduce the background from straight-through molecules into the detector, the machine is equipped with a cold shield located between a chopper wheel and the interaction region and downstream the skimmer. The latter is interfaced to the 10 K stage of a cold head thus reducing the vacuum in the machine to 4×10^{-9} Torr. Two source chambers are located inside the main chamber (Fig. 2); in its current geometry, both beams cross perpendicularly. Each source chamber is pumped by a 2000 and a 430 l s^{-1} maglev pump to the medium 10^{-9} Torr region. A dry roots pump (140 l s^{-1}) roughed by two oil-free EcoDry M30 pumps (16 l s^{-1}) backs the turbo pumps of each source chamber. The supersonic molecular beams of the sources are monitored using a quadrupole mass spectrometer (Extrel). The detector is housed in a separate, triply differentially pumped ultrahigh vacuum chamber (10^{-11} Torr) and is rotatable within the plane defined by both beams. The differ-

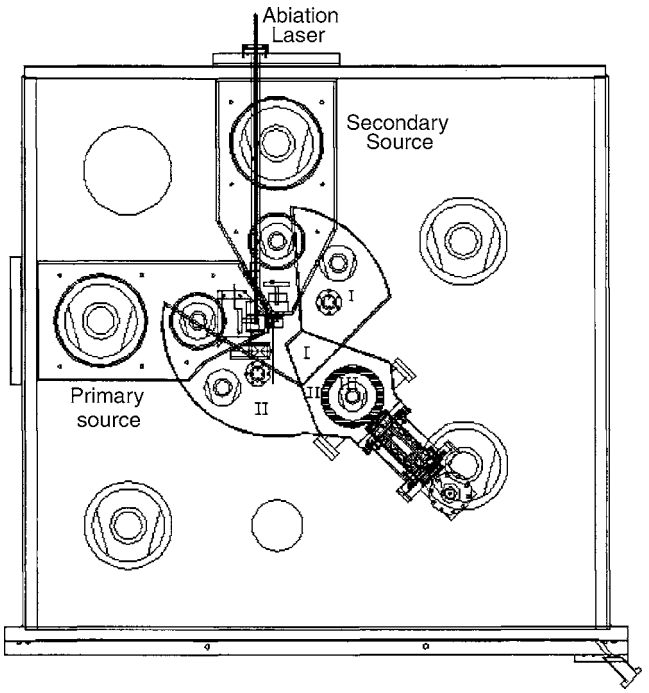

FIG. 2. Top view of the experimental setup with differentially pumped regions I–III and source chambers.

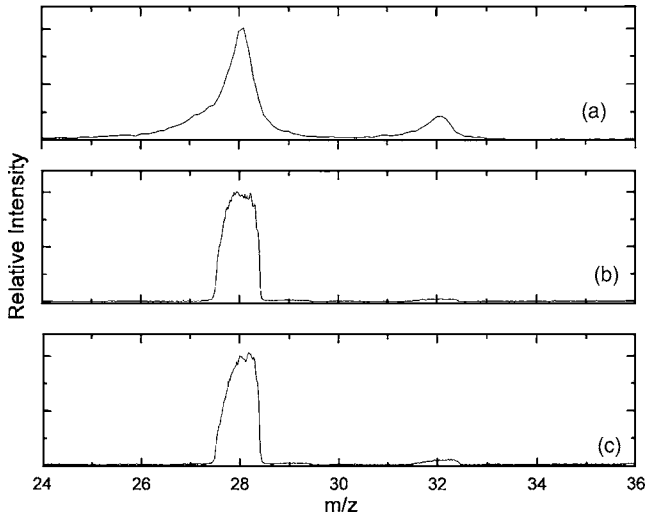

FIG. 3. Partial residual gas spectrum of the ionizer taken at three different parameter sets of the lenses. (a) Extractor: −500 V, filament current: 10 mA, ion energy: 80 eV, and entrance/exit lens: 0 V; (b) extractor: −55 V, filament current: 1 mA, ion energy: 32 eV, and entrance/exit lens: 0 V; and (c) extractor: −150 V, filament current: 2 mA, ion energy: 36 eV, and entrance/exit lens: −140 V. The shape of the mass peaks does not depend on the kinetic energy of the electrons held typically between 80 and 200 eV. The quadrupole housing was grounded; the pre- and postfilters were set to 0 V.

entially pumped detector regions I/II reduce the gas load from the main chamber, whereas region III contains the Brink-type electron impact ionizer,[25] surrounded by a liquid nitrogen cold shield. The quadrupole mass filter and the Daly-type scintillation particle detector[26] are connected to region II. Here, each ion exiting the mass filter hits the surface of a high voltage target (−25 kV) and initiates an electron cascade which is accelerated by the same potential until they reach an organic scintillator whose photon cascade is detected by a photomultiplier (PMT) mounted outside the UHV detector.[27] Each PMT pulse passes a discriminator set at 1.5 mV to eliminate low-level noise and is then converted to a transistor-transistor logic (TTL) signal. The latter is fed into a multichannel scaler (MCS) to record the time-of-flight spectra, i.e., the counts versus the flight time of the ion. Note that each region is pumped by a magnetically levitated turbo molecular pump (430 l s^{-1}); all three pumps are backed by a 430 l s^{-1} turbo molecular pump whose exhaust is connected to an oil-free scroll pump (10 l s^{-1}). This pumping scheme reaches down to the low 10^{-11} Torr in region III; lower pressures can be achieved by operating a cold head inside region III (4 K and 1.5 W). Table I summarized the ions of the residual gases in region III. It is worth mentioning that the performance of the detector strongly depends on the settings

TABLE I. Mass-to-charge (m/z) values and assignment of species observed in the residual gas analyzer mode of our Extrel mass spectrometer. Data were taken with the 1.2 MHz oscillator (1–500 amu). Species at m/z values larger than 44 contribute less than five counts compared to 3000 counts for m/z=28. Thorium and iridium bearing species originate from the filament, copper from the heated copper leads to the ionizer, and iron/nickel/chromium from the heated stainless steel electrodes.

m/z	Assignment	m/z	Assignment	m/z	Assignment	m/z	Assignment
1	$^{1}H^{+}$	17	$^{16}O\ ^{1}H^{+}/^{17}O^{+}$	50	$^{50}Cr^{+}$	64.3	$^{193}Ir^{3+}$
2	$^{1}H_{2}^{+}$	18	$^{1}H_{2}\ ^{16}O^{+}/^{18}O^{+}$	52	$^{52}Cr^{+}$	65	$^{65}Cu^{+}$
3	$^{12}C^{4+}$	20	$^{40}Ar^{2+}$	53	$^{53}Cr^{+}$	77.3	$^{232}Th^{3+}$
4	$^{12}C^{3+}$	28	$^{12}C\ ^{16}O^{+}/^{14}N_{2}^{+}\ ^{56}Fe^{2+}$	54	$^{54}Cr^{+}/^{54}Fe^{+}$	95.5	$^{191}Ir^{2+}$
6	$^{12}C^{2+}$	29	$^{13}C\ ^{16}O^{+}/^{15}N\ ^{14}N^{+}$	56	$^{56}Fe^{+}$	96.5	$^{193}Ir^{2+}$
7	$^{14}N^{2+}$	30	$^{12}C\ ^{18}O^{+}$	57	$^{57}Fe^{+}$	116	$^{232}Th^{2+}$
8	$^{16}O^{2+}$	32	$^{16}O_{2}^{+}$	58	$^{232}Th^{4+}/^{58}Ni^{+}$	124	$^{232}Th\ ^{16}O^{2+}$
12	$^{12}C^{+}$	40	$^{40}Ar^{+}$	60	$^{60}Ni^{+}$	191	$^{191}Ir^{+}$
13	$^{13}C^{+}/^{12}CH^{+}$	44	$^{12}C\ ^{16}O_{2}^{+}$	61	$^{61}Ni^{+}$	193	$^{191}Ir^{+}$
14	$^{14}N^{+}/^{12}CH_{2}^{+}$	45	$^{13}C\ ^{16}O_{2}^{+}$	62	$^{62}Ni^{+}$	232	$^{232}Th^{+}$
15	$^{15}N^{+}/^{12}CH_{3}^{+}$	47.8	$^{191}Ir^{4+}$	63	$^{63}Cu^{+}$	248	$^{232}Th\ ^{16}O^{+}$
16	$^{16}O^{+}/^{12}CH_{4}^{+}$	48.6	$^{193}Ir^{4+}$	63.7	$^{191}Ir^{3+}$	264	$^{232}Th\ ^{16}O_{2}^{+}$

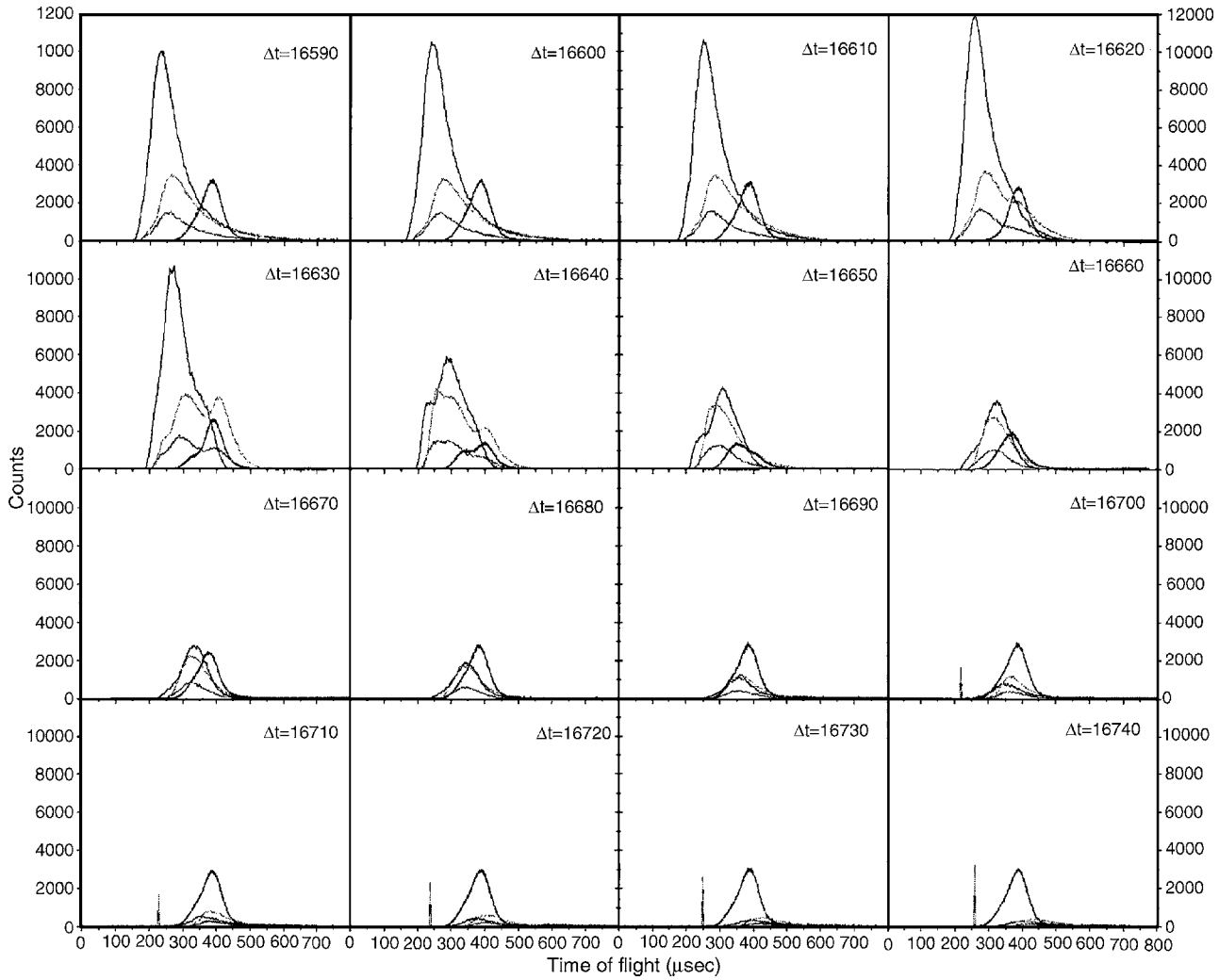

FIG. 4. Time-of-flight spectra of helium seeded ($m/z=4$, blue) atomic carbon ($m/z=12$, black), dicarbon ($m/z=24$, red), and tricarbon ($m/z=36$, green) taken at different delay times between the pulsed valve and the laser. Data were taken with the 2.1 MHz oscillator (resolution: 1 amu mass separation) with 2 mA emission current and a discriminator setting of 1.5 mV.

of potentials of the lenses inside the ionizer (Fig. 3). In improper setting it may require excessive electron emission currents up to 10 mA and large extractor potentials often resulting in broad peaks and hence excessive mass leaking. Potential settings are desirable in which the ionizer is operated with low electron emission currents (<2 mA), low energy ions (10–40 eV), and significantly reduced extractor potentials (<200 V). A slide valve with a Teflon coated O ring is used to separate the main chamber from the first differentially pumped detector region.

IV. CHARACTERISTICS OF THE ABLATION SOURCE

The characterization of the ablation source is carried out first without the chopper wheel unit. Here, an SRS DG535 delay generator is operated at 60 Hz (16 666.66 μs) and defines the time zero ($T0$). The $AB(1)$ output of the pulse generator [50 Ω, +3.5 V, and $B(1)=A(1)+80$ μs] leads to a homemade pulse shaper set at ($C=0.1$ μF), which in turn is connected to the Physik Instumente P-286.23 high voltage pulse amplifier. The output of the amplifier drives the piezoelectric Proch-Trickl valve at repetition rates of 60 Hz, opening times of 80 μs, and a pulse amplitude of −400 V with 4 atm helium (99.9999%) backing pressure. The $A(1)$ output of the pulse generator (TTL, high impedance) passes a frequency divider (division by two and 50 Ω output) fed as an external trigger with a trigger level of +1.0 V to a second pulse generator. The time delayed $AB(2)$ output [$A=T0+16\,666.66$ μs, $B=A+5$ μs, and high impedance TTL pulse] is fed into the SRS 430 multichannel scaler (MCS) utilizing trigger and discriminator levels of +0.5 and +0.2 V. A second output of the frequency divider serves as an external trigger of a third pulse generator (trigger level +1.0 V, and 50 Ω). This unit controls the time sequence of Spectra Physics Nd:YAG (yttrium aluminum garnet) laser (30 Hz, 120 mJ/pulse at 266 nm). Channel $AB(3)$ ($A=T0+X$ μs, $B=A+5$ μs, TTL, and 50 Ω) triggers the flash lamps and $CD(3)$ the Q switch ($C=A+186$ μs, $D=C+5$ μs, TTL, and 50 Ω). Here, X represents the time delay to be optimized. For example, $A=T0+16\,616.66$ μs means that the Q switch will

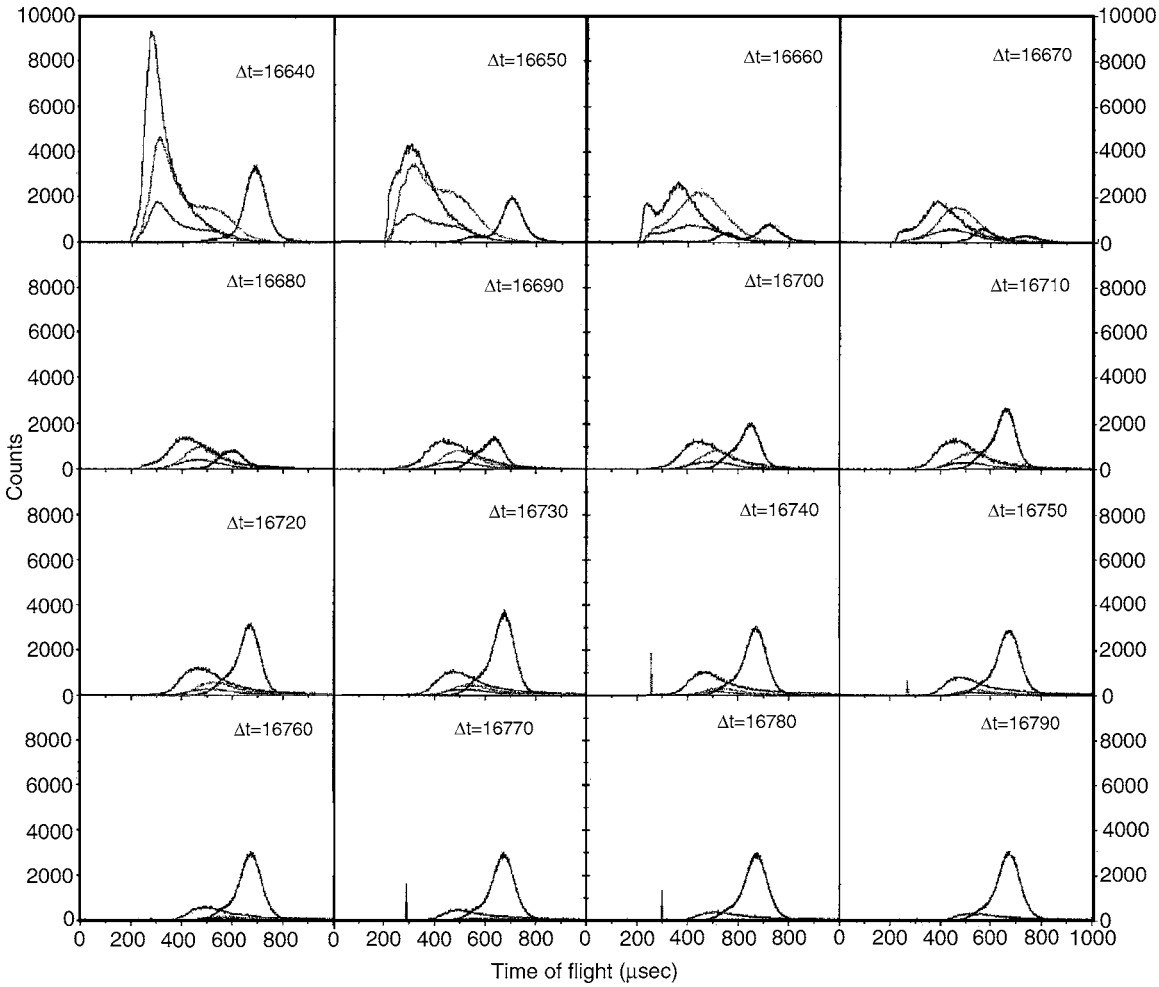

FIG. 5. Time-of-flight spectra of neon seeded ($m/z=20$, blue) atomic carbon ($m/z=12$, black), dicarbon ($m/z=24$, red), and tricarbon ($m/z=36$, green) taken at different delay times between the pulsed valve and the laser. Data were taken with the 2.1 MHz oscillator (resolution: 1 amu mass separation) with 2 mA emission current and a discriminator setting of 1.5 mV.

be triggered 136 μs *after* the trigger pulse to the pulsed valve has been sent out. Note that even if the pulsed valve is triggered with an 80 μs pulse, the time delay in the electronics of about 10 μs, the opening time of 80 μs, and a fall time of about 40 μs to generate the free width half maximum of the gas pulse sumup to about 130 μs. On top of this, the helium atoms have to travel from the nozzle to the laser interaction region; this also takes a few microseconds.

Figures 4 and 5 compile time-of-flight (TOF) spectra of the ablated species (carbon atoms, dicarbon, tricarbon) and the carrier gases taken without the chopper wheel at different time delays X utilizing a 266 nm output of 40 mJ/pulse. The TOF spectra have been taken at an ionizer emission current of 2 mA and electron energy of 80 eV. The data are corrected for the fragmentation pattern of the dicarbon and tricarbon clusters and for the relative ionization cross section.[22] At small delay time of, for instance, 16 590 μs for helium (Fig. 4), the laser is fired only 110 μs after the pulsed valve. As evident from the TOF spectra, the laser fires too early, and the ablated carbon, dicarbon, and tricarbon species are barely seeded in the helium beam. As a matter of fact, changing the delay time from 16 590 down to 16 620 μs alters little in the shape of the TOF data. This presents clear evidence that the ablated species and the noble gas beam do not mix; hence, that the time delay is not a correct one. Even switching off the pulsed valve hardly changes the TOF profiles of the ablated species suggesting that we are in the "free ablation mode" of the source. As the delay time rises further beyond 16 630 μs, the change in peak shape is evident, and the ablated species are seeded inside the noble carrier gas. Note, however, that the delay time window in which the ablation source can be operated properly has also upper limits. Let us have a close look at the delay time of, for instance, 16 690 μs. Here, the laser fires 210 μs after the pulsed valve. Considering the opening and closing time of the pulsed valve of 160 μs and the electronic offset, the laser is fired after the gas pulse crossed the actual ablation region. Therefore, the ablated carbon species hit the gas pulse and are self-attenuated. In case of neon (Fig. 5), the delay time window can be also optimized optically. Here, orange glow patterns are visible inside the source chamber once the laser pulse and the neon gas pulse cross. Summarized, operating the ablation source with helium and neon carrier gases sug-

TABLE II. Typical delay times, peak velocities (v_p), and speed ratios (S) of supersonic dicarbon beams. The speed ration is defined via Eq. (1) with $\alpha = [(2RT)/m]^{-1/2}$, with m being the mass of the species, R the ideal gas constant, and T the temperature of the beam.

Carrier gas	Pulsed valve delay	Laser delay	v_p (ms^{-1})	S
Ne	$A(1)=T0+1860$ μs	$A(3)=T0+16\,635$	1060±17	4.7±0.5
He	$A(1)=T0+1875$ μs	$A(3)=T0+16\,632$	1629±6	5.2±0.1
He	$A(1)=T0+1876$ μs	$A(3)=T0+16\,645$	1956±23	5.7±0.2
He	$A(1)=T0+1890$ μs	$A(3)=T0+16\,638$	2362±42	4.9±0.3
He	$A(1)=T0+1890$ μs	$A(3)=T0+16\,640$	2608±36	4.1±0.2

gests a practical delay time window of 16 630–16 645 μs, i.e., firing the laser 150–165 μs after the pulsed valve trigger.

So far, we have not utilized the chopper wheel in our experimental setup. However, since the ablation beam is pulsed, each part of the pulsed beam holds a distinct peak velocity of the reacting species. Also, the nonchopped ablation beam can contain metastable species such as electronically excited carbon atom and vibrationally excited dicarbon and tricarbon molecules. Therefore, it is advisable to incorporate a four-slotted chopper wheel operated at 120 or 240 Hz between the skimmer of the primary source and the oxygen-free high conductivity (OFHC) copper shield. An infrared diode is attached to the top of the chopper unit and provides the time zero of the experiments. By selecting the time delay between the diode pulse and the pulsed valve, distinct parts of the ablation pulse can be selected. Table II compiles the delay time conditions, peak velocities, and speed ratio of supersonic dicarbon beams at typical examples. Here, we achieved stable peak velocities between 800 and 3800 m s^{-1} and speed ratios S of up to 6. Likewise, the number density of the reagent species in the interaction region is increased by a factor of 3–4 compared to an earlier version of this ablation source thus providing up to 3×10^{13} cm^{-3} reactant species,

$$N(v) = v^2 \exp\left[-\left(\frac{v}{\alpha} - S\right)^2\right]. \quad (1)$$

Finally, we would like to comment briefly on the ionizer setting and laser output power in our experiments. Figure 6 depicts TOF spectra of dicarbon beam taken at different emission currents of the electron impact ionizer between 5 and 1 mA [parameter set (c), Fig. 3]. At larger emission currents, the TOF spectra have a long tail which decreases as the emission current is being reduced from 5 to 2 mA. On the other hand, reducing the current down to 1 mA does not change the TOF patterns. These data suggest that at higher emission currents, space charge effects of the generated ions

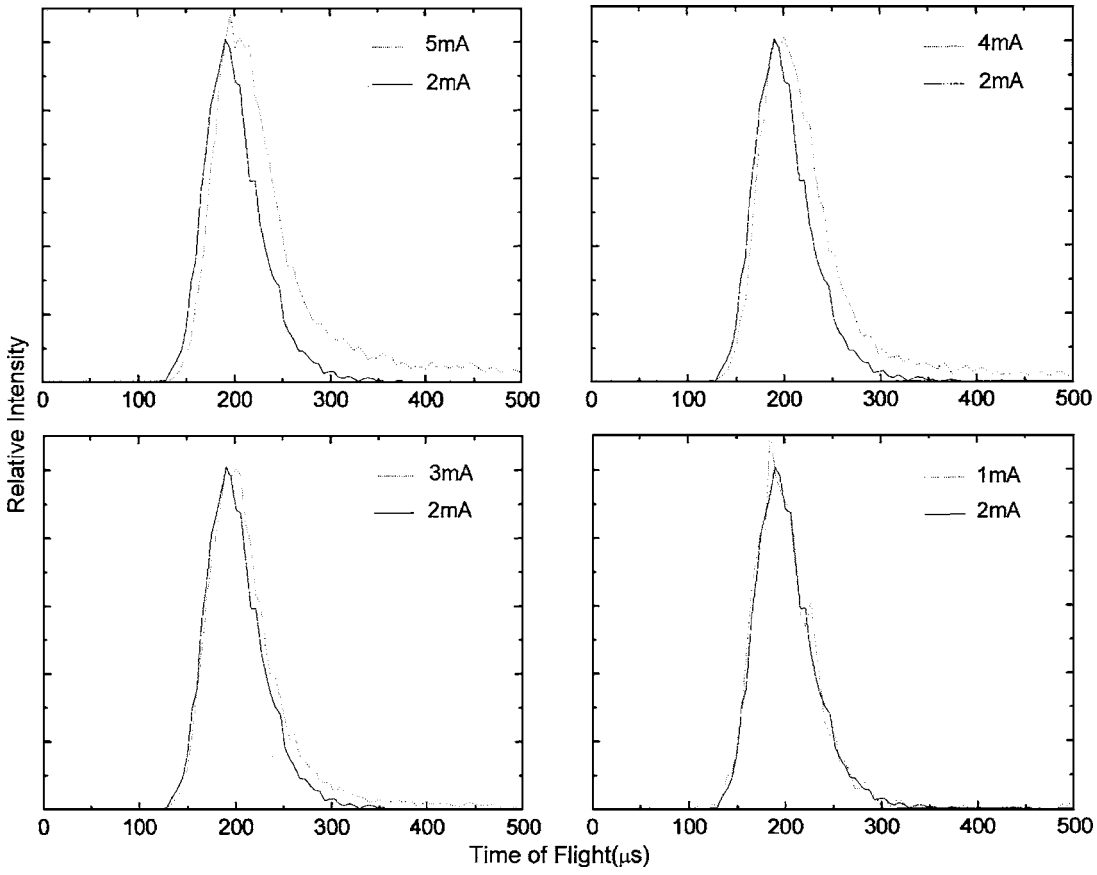

FIG. 6. Time-of-flight spectra of the dicarbon beam ($m/z=24$) recorded at different emission currents of the electron impact ionizer utilizing parameter set (c) from Fig. 3. TOF spectra have been normalized for intensity.

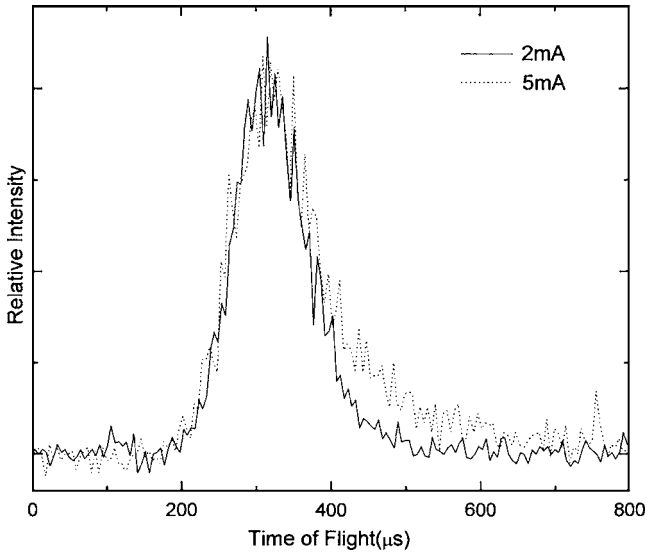

FIG. 7. Time-of-flight spectrum of the butadiynyl radical C_4H (m/z=49) recorded at two emission currents of the electron impact ionizer at 2 mA (solid line) and 5 mA (dashed line).

are present. To confirm this hypothesis, we crossed a dicarbon beam with a pulsed acetylene beam (C_2H_2, 550 Torr backing pressure) and detected the butadiynyl radical $C_4H(X\,^2\Sigma^+)$ under single collision conditions at m/z=49. Time-of-flight spectra of the radical were recorded at the center-of-mass angle (31°) (Fig. 7) at two emission currents of 5 and 2 mA. The findings of the crossed beam experiments mirror the patterns of the on-axis dicarbon beam characterization and suggest that the ionizer should not be operated at emission currents beyond 2 mA if parameter set (c) is utilized.

ACKNOWLEDGMENTS

This work was supported by the US Department of Energy-Basic Energy Sciences (DE-FG02-03ER15411) for two of the authors (X.G. and R.I.K.) and by the National Science Foundation (CHE-0234461) for two of the authors (Y.G. and R.I.K.).

[1]Combustion Chemistry: Elementary Reactions to Macroscopic Processes, University of Leeds, United Kingdom, 9–11 January 2001 [Faraday Discuss. **119** (2002)].
[2]R. D. Kern, H. Chen, J. H. Kiefer, and P. S. Mudipalli, Combust. Sci. **85**, 77 (1992); M. Frenklach, Phys. Chem. Chem. Phys. **4**, 2028 (2002); C. E. Baukal, *Oxygen-Enhanced Combustion* (CRS, New York, 1998); A. G. Gordon, *The Spectroscopy of Flames* (Wiley, New York, 1974).
[3]P. John, J. R. Rabeau, and J. I. B. Wilson, Diamond Relat. Mater. **11**, 608 (2002).
[4]J. Appel, H. Bockhorn, and M. Frenklach, Combust. Flame **121**, 122 (2000); A. Kazakov and M. Frenklach, *ibid.* **14**, 484 (1998); **112**, 270 (1998); L. Vereecken, H. F. Bettinger, and J. Peeters, Phys. Chem. Chem. Phys. **4**, 2019 (2002); H. Richter and J. B. Howard, Prog. Energy Combust. Sci. **26**, 565 (2000).
[5]A. Kazakov and M. Frenklach, Combust. Flame **112**, 270 (1998).
[6]C. Baird, *Environmental Chemistry* (Freeman, New York, 1999).
[7]B. J. Finlayson-Pitts and J. N. Pitts, Science **276**, 1045 (1997).
[8]R. P. Wayne, *Chemistry of the Atmosphere* (Oxford University Press, Oxford, 2000).
[9]A. Necula and L. T. Scott, J. Am. Chem. Soc. **122**, 1548 (2000).
[10]R. Taylor, G. J. Langley, H. W. Kroto, and D. R. M. Walton, Nature (London) **366**, 728 (1993).
[11]F. Battin-Leclerc, Phys. Chem. Chem. Phys. **4**, 2072 (2002); H. Richter and J. B. Howard, *ibid.* **4**, 2038 (2002); M. Frenklach, *ibid.* **4**, 2028 (2002).
[12]A. G. Gordon, *The Spectroscopy of Flames* (Chapman and Hall, London/Wiley, New York, 1974).
[13]N. S. Goroff, Acc. Chem. Res. **29**, 77 (1996); K. H. Homann, Angew. Chem., Int. Ed. **37**, 2434 (1998).
[14]M. F. Budyka, T. S. Zyubina, A. G. Ryabenko, V. E. Muradyan, S. E. Esipov, and N. I. Cherepanova, Chem. Phys. Lett. **354**, 93 (2002); Y.-T. Lin, R. K. Mishra, and S.-L. Lee, J. Phys. Chem. B **103**, 3151 (1999).
[15]T. Shiomi, H. Nagai, K. Kato, M. Hiramatsu, and M. Nawata, Diamond Relat. Mater. **10**, 388 (2001).
[16]S. A. Redman, C. Chung, K. N. Rosser, and M. N. R. Ashfold, Phys. Chem. Chem. Phys. **1**, 1415 (1999); J. S. Foord, K. P. Loh, N. K. Singh, R. Z. B. Jackman, and G. J. Davies, J. Cryst. Growth **164**, 208 (1996).
[17]A. G. Loewe, A. T. Hartlieb, J. Brand, B. Atakan, and K. Kohse-Hoeinghaus, Combust. Flame **118**, 37 (1999).
[18]A. N. Goyette, Y. Matsuda, L. W. Anderson, and J. E. Lawler, J. Vac. Sci. Technol. A **16**, 337 (1998).
[19]G. Pascoli and A. Polleux, Astron. Astrophys. **359**, 799 (2000); N. Herlin, I. Bohn, C. Reynaud, M. Cauchetier, A. Galvez, and J.-N. Rouzaud, *ibid.* **330**, 1127 (1998).
[20]H. G. M. Hill, A. P. Jones, and L. B. d'Hendecourt, Astron. Astrophys. **336**, L41 (1998).
[21]A. C. Andersen, U. G. Jorgensen, F. M. Nicolaisen, P. G. Sorensen, and K. Glejbol, Astron. Astrophys. **330**, 1080 (1998).
[22]R. I. Kaiser and A. G. Suits, Rev. Sci. Instrum. **66**, 5405 (1995).
[23]W. D. Geppert, C. Naulin, and M. Costes, Chem. Phys. Lett. **333**, 51 (2001).
[24]D. Proch and T. Trickl, Rev. Sci. Instrum. **60**, 713 (1989).
[25]G. O. Brink, Rev. Sci. Instrum. **37**, 857 (1966).
[26]N. R. Daly, Rev. Sci. Instrum. **31**, 264 (1960).
[27]X. Gu, Y. Guo, E. Kawamura, and R. I. Kaiser, Rev. Sci. Instrum. **76**, 083115 (2005).